Kinetic and Dynamic Aspects of Lifetime Oscillations in the Predissociation of Hydrogen Chloride Ions †

ARTICLE *in* THE JOURNAL OF PHYSICAL CHEMISTRY A · APRIL 2006

Impact Factor: 2.69 · DOI: 10.1021/jp054365n · Source: PubMed

2 AUTHORS, INCLUDING:

M. V. Korolkov
National Academy of Sciences of Belarus
66 PUBLICATIONS **709** CITATIONS

SEE PROFILE

Kinetic and Dynamic Aspects of Lifetime Oscillations in the Predissociation of Hydrogen Chloride Ions†

Mikhail V. Korolkov‡,§ and Karl-Michael Weitzel*,§

Stephanov Institute of Physics, National Academy of Science, Scarina ave. 70, 220602 Minsk, Republic of Belarus, and Fachbereich Chemie, Philipps Universität Marburg, Hans Meerwein Strasse, 35032 Marburg, Germany

Received: August 5, 2005; In Final Form: September 27, 2005

The predissociation dynamics of hydrogen chloride ions (HCl^+ and DCl^+) in the electronic A $^2\Sigma^+$ state has been investigated by solving the time dependent Schrödinger equation. The predissociation lifetime is shown to strongly depend on the vibrational and the rotational quantum number, with quasi-periodic oscillations. Rovibronic states, which exhibit lifetimes about 1 order of magnitude larger than those of neighboring states, are termed rotational islands of stability (RIS). These RIS can be correlated with characteristic reference energies, e.g., the difference between rovibronic eigenenergy and the energy of crossing of rotronic bound and repulsive potentials. The origin of these RIS is illustrated by model studies of the positions of the nuclear wave functions involved.

I. Introduction

The struggle for precise rate constants in gas phase reaction kinetics still poses one of the important challenges in atmospheric chemistry.[1,2] Often the incompleteness of our understanding is related to the limited accuracy of thermochemical data, e.g., bond energies and heats of formation, as in the case of the hydroxyl radical. In general, the kinetics and the dynamics of a chemical process are just different aspects of the same process. Combining these aspects requires the understanding of coherence effects in the dynamics of transient species.[3] Thus, the dynamical behavior of transient intermediate states constitutes the key to understanding a majority of elementary processes in chemistry, but also in physics and biology.[4−6] The question of coherence in transition states is also connected to the prospect of controlling the outcome of chemical reactions.[7−10] Again, a better understanding of the transition from kinetics to dynamics will open access to such control strategies. In the context of fast photochemical processes this includes not only the rearrangement of nuclear coordinates but also the transfer of population between molecular states and interference effects associated with this.

In the current work we are dealing with kinetical and dynamical aspects of predissociation in small molecular ions. Important features are the eigenstates of the molecule, its quantum resolved dissociation threshold, E_o,[11] and the lifetime of states above E_o.[12] With respect to predissociation lifetime pioneering work was based on the Fermi−Wentzel golden rule.[13−22] That approach is inherently based on stationary vibrational Schrödinger equations. A more sophisticated approach involves the investigation of real time dynamics by, e.g., solving the time dependent Schrödinger equation.[23−26]

In previous work we have investigated the time dependent Schrödinger equation for the predissociation dynamics of HCl^+ and HBr^+.[27,28] The following interesting phenomena became eminent: In the case of free decay of an isolated reactive state, this decay follows monoexponential characteristics. This is in general equivalent to first-order kinetics. However, in the case of multichannel interactions or redistribution of population the decay may exhibit multiexponential features not easily translated into a single rate constant.[27] A more general discussion would have to include dissipation from the first-order state, which affects the time domain−frequency domain relation.

Predissociation processes are inherently subject to interference effects between wave functions of a quasi bound state and that of the dissociation continuum. This leads to the situation that population may be trapped behind an effective barrier although it has sufficient energy to overcome it. This effect has been known for predissociating vibrational states and is, e.g., the reason for increasing lifetime with increasing vibrational quantum number for certain regions in the vibrational predissociation of HX^+ ions.[29,30] In previous work from our group we have shown that interference effects also occur for predissociating rovibrational states. There exist specific rotational states for which the lifetime is an order of magnitude larger than that of neighboring states.[31] We nicknamed these states "rotational islands of stability" (RIS). These RIS appear to be associated with quasi-periodic lifetime oscillations.

The goal of the current work is to present a deeper investigation of these lifetime oscillations, their periodicity, and their contrast. Here, it is instructive to investigate the role of molecule specific properties, which can, e.g., be tackled by looking at different isotopomers of the hydrogen chloride ion, i.e., HCl^+ and DCl^+. Ultimately, the analysis comes back to the pivotal aspect of the relation between dynamics and kinetics. From the methodological point of view it is interesting to compare the free decay of predissociating molecules with optically driven predissociation dynamics.

II. Computational Techniques

In the current work predissociation lifetimes of HCl^+ and DCl^+ ions have been derived by numerical solution of time dependent, coupled Schrödinger equations. Details of the

† Part of the special issue "Jürgen Troe Festschrift".
‡ National Academy of Science.
§ Philipps Universität Marburg.

10.1021/jp054365n CCC: $33.50
Published on Web 11/01/2005

approach have been described in previous papers.[27,28,31] Only the details specific to the current work will be outlined below.

As in previous work the input used for the wave packet calculations is based on ab initio data from Dalgarno et al.[32] However, we decided to slightly adjust the ab initio potential data to better fit known spectroscopic parameters in the stable region below the onset of predissociation.[11,29] To be able to compare the dynamics of HCl^+ and DCl^+, we therefore had to repeat some calculations for the HCl^+ ion. For illustration, the relevant rotronic (rotational + electronic) potential curves are shown in Figure 1. The predissociation of HCl^+ and DCl^+ molecular ions in the A $^2\Sigma^+$ electronic state is caused by spin−orbit coupling to the three nominally repulsive electronic states, $^4\Sigma^-$, $^2\Sigma^-$, and $^4\Pi$ (listed in order of increasing energy at the equilibrium distance!)

As indicated in Figure 1, the current work takes into account five different electronic states: (i) the ion ground state (X $^2\Pi_{3/2}$, $j = 1$), (ii) the first excited electronic state (A $^2\Sigma^+$, $j = 2$), and (iii) three repulsive states, $^4\Sigma^-$ ($j = 3$), $^2\Sigma^-$ ($j = 4$) and $^4\Pi$ ($j = 5$). For these states coupled Schrödinger equations have been set up as given below:

$$i\hbar \frac{\partial \Psi_X(r,t)}{\partial t} = [\hat{T} + \tilde{V}_X]\Psi_X(r,t) + \eta_{XA}(r)\, E_z(t)\, \Psi_A(r,t) + \eta_{X4}(r)\, E_z(t)\, \Psi_4(r,t) \quad (1)$$

$$i\hbar \frac{\partial \Psi_A(r,t)}{\partial t} = [\hat{T} + \tilde{V}_A]\Psi_A(r,t) + \eta_{AX}(r)\, E_z(t)\, \Psi_X(r,t) + \sum_{j=3}^{5} H^{so}_{A,j}(r)\, \Psi_j(r,t) \quad (2)$$

$$i\hbar \frac{\partial \Psi_3(r,t)}{\partial t} = [\hat{T} + \tilde{V}_3]\Psi_3(r,t) + H^{so}_{A,3}(r)\, \Psi_A(r,t) \quad (3)$$

$$i\hbar \frac{\partial \Psi_4(r,t)}{\partial t} = [\hat{T} + \tilde{V}_4]\Psi_4(r,t) + \eta_{X,4}(r)\, E_z(t)\, \Psi_X(r,t) + H^{so}_{A,4}(r)\, \Psi_A(r,t) \quad (4)$$

$$i\hbar \frac{\partial \Psi_5(r,t)}{\partial t} = [\hat{T} + \tilde{V}_5]\Psi_5(r,t) + H^{so}_{A,5}(r)\, \Psi_A(r,t) \quad (5)$$

where the potential energy in the relevant electronic states is given by

$$\tilde{V}_X = V_X + \frac{J_X(J_X+1) - \Omega_X^2}{2\mu r^2} \quad (6)$$

$$\tilde{V}_A = V_A + \frac{N_A(N_A+1)}{2\mu r^2} + 0.5\gamma N_A \quad (7)$$

$$\tilde{V}_j = V_j + \frac{J_j(J_j+1) - \Omega_j^2}{2\mu r^2} \quad \text{for } j = 3\ (^4\Sigma^-),\ 4\ (^2\Sigma^-),\ \text{and } 5\ (^4\Pi) \quad (8)$$

V_X, V_A, and V_j are the ab initio potential energies of the X, A, and the three repulsive states, respectively, to which the appropriate rotational energy is added. Here we use $J_X = N_A + 1.5$ (P_1 transition), $J_j = N_A + 0.5$, $\gamma(HCl^+) = 0.51$ cm^{-1}, and $\gamma(DCl^+) = 0.25$ cm^{-1}. Note that for the ground electronic X state and the repulsive $^4\Sigma^-$, $^2\Sigma^-$, and $^4\Pi$ states, Hund's case a representation was chosen, for the A state Hund's case b applies. The data shown in Figure 1 are for DCl^+ with $N_A = 61$. For the bound, ground state $\Omega_X = 1.5$; for the three repulsive states $\Omega_j = 0.5$. The reduced masses are $\mu(H^{35}Cl^+) = 1785.68$ au (au = atomic units) and $\mu(D^{35}Cl^+) = 3542.23$ au. In general, the five states (and thus the Schrödinger equations) are coupled via spin−orbit interaction, $H^{so}_{A,j}(r)$, and—if taken into account—through optical excitation, e.g., $\eta_{XA}(r)\, E_z(t)$, where $\eta_{XA}(r)$ is the transition dipole moment connecting states X and A. The radial dependence of the latter is taken into account. Note that the model is based on HCl^+ ions oriented along the x axis. The spin−orbit coupling matrix elements were taken from Korolkov et al.[28] The optical excitation will be discussed below.

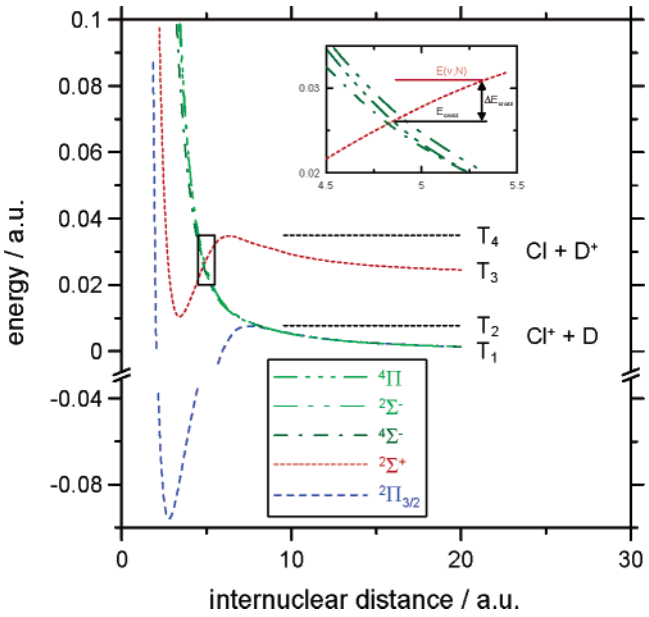

Figure 1. Rotronic potential curves ($N_A = 61$) of the DCl^+ ion relevant for the predissociation dynamics, based on data from Dalgarno et al.[32] The inset shows an enlarged view of the crossing region (also marked by a box in the main figure).

The laser field was represented by the following function (cf. section III.2):

$$E(t) = \begin{cases} \sin^2\left[\frac{\pi t}{t_l}\right] \sin(\omega t) & \text{for } 0 \le t \le t_l \\ 0 & \text{for } t > t_l \end{cases} \quad (9)$$

where t_l is characterizing the width of the laser pulse at the base. Typically, $t_l = 80$ ps was chosen in this work.

The five nuclear wave functions are represented on an equidistant N-point spatial grid with $r = (r_1, r_2, ..., r_N)$, $r_1 = 1.5\ a_o$, $\Delta r = 0.02\ a_o$, for $4096 < N < 32768$. A combination of the split-operator method[33] and the integral equation method[34,35] is used for the propagation of the wave functions (given in eqs 1−5) in time with time steps of $\Delta t \le 1$ atomic unit (1 au ≈ 0.024 fs). The total propagation time (identical to the laser pulse duration) is always chosen as appropriate for the corresponding fragmentation dynamics. Typically, this total time is about 1 order of magnitude larger than the respective lifetime. This ensures that the line widths derived do not depend on the laser pulse duration. The absorbing boundary[36] is used to prevent the artificial reflection of all $\Psi_j(r,t)$ wave functions at the edge of the grid, where necessary.

From the methodological point of view various different situations, in which an excited state wave function may decay, are considered in this work:

i. The free decay of a zero-order wave function. For this approach the population is put into the excited bound state at time zero before switching on the spin−orbit coupling.

ii. The decay of a wave function in a laser field. For this approach optical excitation starting from the ion ground state is taken into account by means of a realistic laser pulse. Spin−orbit coupling is taken into account from the beginning.

Clearly case ii is relevant for any comparison with spectroscopic photodissociation experiments.[11,12,37,38] Case i, however, has the advantage of significantly reduced computational efforts. The question addressed in this work is, how large indeed is any possible difference in the dynamics between cases i and ii? In case ii direct optical coupling is only taken into account between states A and X and $^2\Sigma^-$ and X, respectively. Spin−orbit coupling is only taken into account between the A state and the three repulsive states, but not between the A state and the X state. The latter would be relevant if we considered emission processes, which is not the case.

As it turns out, five different characteristic energies are most relevant to the photochemical process of HCl^+ (DCl^+). T_1 is the thermodynamic threshold for fragmentation, i.e., the predissociation threshold. Because T_1 is also the dissociation limit of the X state, formation of fragments is physically not possible below T_1. Note that T_1 correlates with the formation Cl^+ ions. Predissociation is the only fragmentation process between T_1 and T_3. T_2 is the top of a centrifugal barrier induced by the rotational angular momentum N_X of the molecular ion. E_{cross} (cf. insert of Figure 1) is the zero-order crossing between the bound A $^2\Sigma^+$ state and the repulsive $^4\Pi$ state. In principle, there are three different crossing energies because there are three repulsive states. However, for simplicity we will mainly refer to the crossing with one repulsive state throughout the text. The important fact is the energy of this crossing point depends on the rotational angular momentum of the molecular ions. However, its position in the internuclear distance domain does not significantly change with N. T_3 is the thermodynamic threshold for direct dissociation, which correlates with the formation of D^+ ions. Indeed, the fact that predissociation and direct dissociation lead to different ions, easily distinguishable in a mass spectrometer, is an intriguing aspect of the specific molecular system chosen. Finally, T_4 is the top of a centrifugal barrier for direct dissociation. Note that T_3 and T_4 coincide in the case of rotational quantum number $N_A = 0$ (as well as T_1 and T_2, respectively, for $N_X = 0$). Another energetic quantity pivotal to the current work is ΔE_{cross}, the energy difference between a given rovibronic energy, $E(v,N)$, and the zero-order crossing, E_{cross} (cf. Figure 1).

III. Results

III.1. Kinetic Aspects of Free Decay of "Eigenstates". III.1.1. DCl. In this section we first describe results of the free decay of a rovibrational "eigenfunction". These calculations do not take into account the optical excitation from the ion ground state X, i.e., $E_z(t) = 0$, but rather start with $|\Psi_A(r,t=0)|^2 = 1$; i.e., the population is placed into the A state at time zero.

We first discuss the first vibronic state above the predissociation threshold in DCl^+, the $v_A = 10$ state.[12] For this vibrational state experimental and theoretical evidence indicates that all rotational states lie above the predissociation threshold. For the rotational ground state $N_A = 0$ the calculated lifetime τ turns out to be larger than the reliable upper limit of our calculation, which is about 5 ps. The calculated value of τ is very sensitive to details of the potential curve, which are beyond the accuracy of the ab initio data available. We emphasize that the exact value of τ is not the aim of this paper. Rather, we are interested in the variation of τ with the rotational angular momentum N. With increasing rotational quantum number in $v_A = 10$ the lifetime decreases significantly. For $N_A = 10$ the lifetime has dropped to about 4.3 ps. The general trend of decreasing lifetime is in qualitative agreement with experimental information, although the actual values differ.[12] Between $N_A = 25$ and $N_A = 35$ the lifetime reaches a minimum on the order of 100 fs. For even higher rotational quantum numbers the lifetime increases again. For $N_A = 39$ the lifetime reaches a maximum. Above $N_A = 39$ the lifetime decreases again, runs through a minimum around $N_A = 45$, increases again, runs through a second maximum for $N_A = 50$ and decreases again. In accordance with previous work, the two maxima in the lifetime are termed "rotational islands of stability" (RIS).[31] These RIS will be more deeply investigated in the following part of the work. We emphasize that the decay of the wave functions basically follows an exponential law. Thus the dynamical time evolution could well be represented by a classical first-order kinetic model. Next we demonstrate that the RIS also occurs for other vibrational states within the A state.

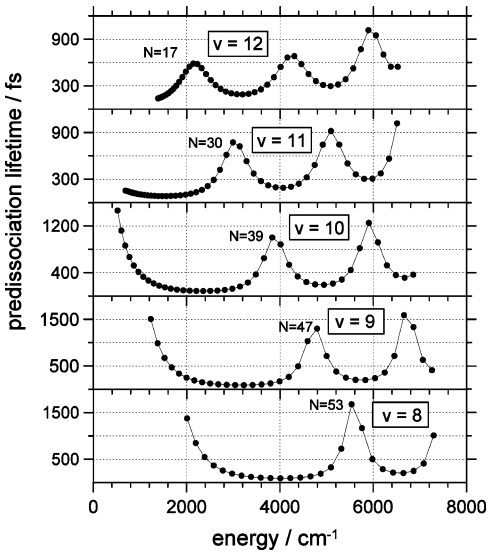

Figure 2. Predissociation lifetime of DCl^+ in the $v_A = 8-12$ states as a function of the rotational energy relative to the predissociation threshold.

Figure 2 shows a plot of the predissociation lifetime of DCl^+ in several vibrational states. Here, we plot these lifetimes as a function of the rotational energy, rather than the rotational quantum number discussed above. This has the advantage that systematic trends will become obvious, which would not be the case in a τ vs N representation. The rotational energy is referenced to the threshold T_1, i.e., the thermodynamic limit for formation of fragments.

From Figure 2 it is evident that the RIS are a general phenomenon, which appear in all vibrational states investigated (including the $v_A = 10$ state discussed above). In most vibrational states two RIS appear, in the $v_A = 12$ state even three. More specifically, the RIS occur for the following rovibronic states, where the corresponding predissociation lifetimes are given in brackets: $v_A = 8$, $N_A = 53$ (1679 fs); $v_A = 9$, $N_A = 47$ (1300 fs) and 56 (1590 fs); $v_A = 10$, $N_A = 39$ (1003 fs) and 50 (1254 fs); $v_A = 11$, $N_A = 30$ (773 fs) and 43 (919 fs); $v_A = 12$, $N_A = 17$ (587 fs) and 35 (682 fs) and 45 (1016 fs).

It is interesting to note that the threshold for direct dissociation, T_3, occurs at 5094 cm^{-1} (0.02321 au). All data points

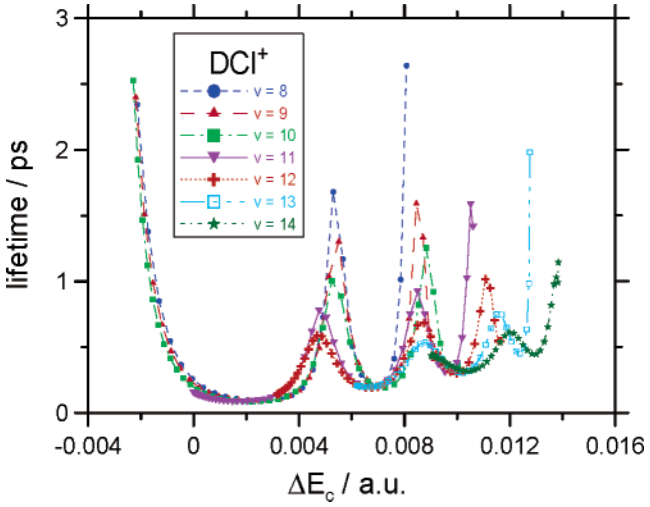

Figure 3. Predissociation lifetime of DCl^+ in the $\upsilon_A = 8-12$ states as a function of the energy difference between the rovibronic dissociating state and the zero-order crossing of the rotronic states.

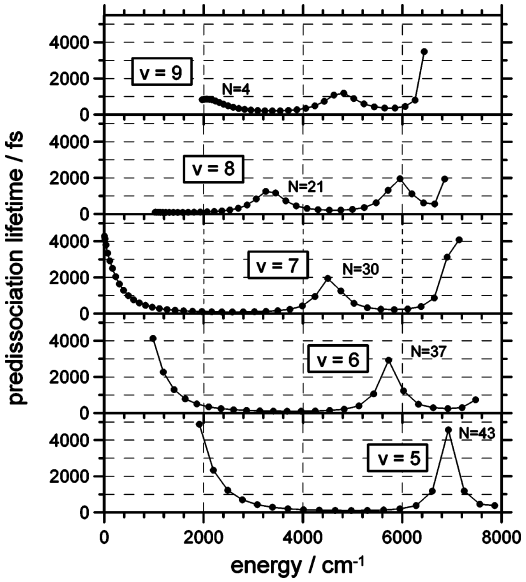

Figure 4. Predissociation lifetime of HCl^+ in the $\upsilon_A = 5-9$ states as a function of the rotational energy relative to the predissociation threshold.

included in Figure 2 are below the top of the centrifugal barrier for direct dissociation, T_4, which occurs at 7624 cm^{-1} (0.034738 au) for $N_A = 61$. Between thresholds T_3 and T_4 direct dissociation is possible by tunneling. However, we found that tunneling is only important (yield >1%) for states very close to T_4. The competition between predissociation and direct dissociation will be discussed elsewhere.[39] Only states for which the yield of direct dissociation is smaller than 1% are included in the current work. Although we emphasized that absolute lifetimes are not the concern of this work, we point out that the experimental lifetimes for the $\upsilon_A = 11$ and $\upsilon_A = 12$ state, are 89 and 76 fs, respectively.[12] The calculated values of this work are 153 and 139 fs, respectively, thus showing the same trend of decreasing τ with increasing υ.

Evidently there appear to be regularities in these RIS. For example, there is a regularity in the shift of the position of, e.g., the first RIS when going from $\upsilon_A = 8$ to $\upsilon_A = 12$. Also, there is a periodicity in the RIS; i.e., the energy distance of first and second RIS is very similar for different vibrational states. Within one vibrational state the maximum lifetime increases when going from the first to the second RIS. At the same time the width of the RIS becomes smaller. In the following we attempt to resolve the physical origin of these regularities (see also Figure 3 of ref 31).

The results discussed above indicate that a different representation of the lifetime results may be helpful, i.e., a representation on a common energy scale for all vibrational states. A helpful energy reference turns out to be the energy where the zero-order rotronic states cross (cf. Figure 1). As pointed out earlier, this crossing energy slightly depends on the repulsive state chosen (the energy difference between the highest and the lowest crossing point is about 300 cm^{-1}). We also note that different channels dominate the predissociation for different rovibrational states. Here, we have chosen the crossing between the A $^2\Sigma^+$ state and the $^4\Pi$ state as the reference. The crossing with the $^4\Sigma^-$ state is about 100 cm^{-1} lower in energy, and that with the $^2\Sigma^-$ state about 200 cm^{-1} higher in energy. This new representation is shown in Figure 3. Plotting the lifetimes referenced to one of the other crossing energies would simply shift the graph in relative energy.

Evidently, several RIS occur at very similar ΔE_c values in consecutive vibrational states. More specifically, the first RIS occurs for nearly the same ΔE_c in $\upsilon_A = 8$ and 9. For $\upsilon_A = 10-12$ the position of the first RIS moves toward smaller ΔE_c values. The average position of this first RIS is at about $\Delta E_c \approx 0.005$ au. The fact that the RIS do not occur at identical ΔE_c values most likely correlates with the existence of three channels contributing to this predissociation. For $\upsilon_A = 9$ to $\upsilon_A = 13$ another RIS is observed around $\Delta E_c \approx 0.0085$ au. This RIS occurs at nearly the same ΔE_c for all vibrational states. A third RIS is observed for $\upsilon_A = 13$ and 14 (and less clear for $\upsilon_A = 12$) around $\Delta E_c \approx 0.0115$. Here, the third RIS for $\upsilon_A = 14$ occurs at slightly higher relative energy than that for $\upsilon_A = 13$. The average energetic distance between first and second RIS and second and third RIS is about 0.0035 au and 0.003 au, respectively. For the first RIS there seems to be a trend toward slightly smaller ΔE_c values with increasing υ_A. For the third RIS the trend indicates larger ΔE_c values with increasing υ_A. The position of the intermediate second RIS is almost independent of the vibrational state. The fastest decay is observed slightly above the energy $\Delta E_c = 0.0116$ with about 80 fs. The line connecting the regions of minimum lifetime shows a positive slope; i.e., the minimum lifetime increases with increasing ΔE_c.

III.1.2. HCl. To better understand the molecular origin of the RIS, it is helpful to compare the results obtained for DCl^+ with those for its isotopomer HCl^+. Predissociation lifetimes of the HCl^+ have also been presented in earlier work.[31] However, the calculations of the current work are based on slightly improved potential energy curves compared to previous work, such that recalculation was considered to be necessary.

From experiments it is known that the predissociation threshold in HCl^+ occurs in the $\upsilon_A = 7$ manifold between the rotational states $N_A = 0$ and $N_A = 1$.[11] For the higher vibrational states all rotational states predissociate.[12] For the lower vibrational states rotational states predissociate above a certain rotational quantum number. Calculated predissociation lifetimes are presented in Figure 4 for the vibrational states $\upsilon_A = 5$ to $\upsilon_A = 10$. We first discuss the $\upsilon_A = 9$ state. For this vibrational state the calculated lifetime at threshold is about 4 ps. Again the exact value is very sensitive to details of the potential curves, which are beyond the accuracy of the current ab initio data. Above the predissociation threshold in the $\upsilon_A = 7$ state the predissociation lifetime first decreases with increasing rotational energy. For $N_A = 7$ the calculated lifetime is about 800 fs. This

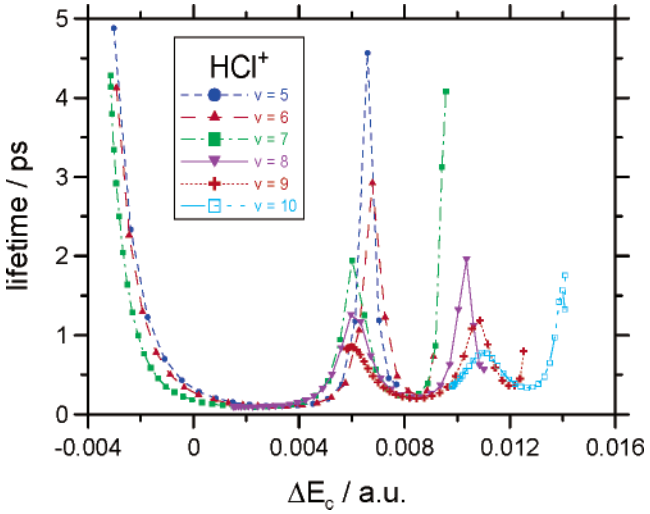

Figure 5. Predissociation lifetime of HCl^+ in the $v_A = 5-10$ states as a function of the energy difference between the rovibrational state and the zero-order crossing of the rotronic potentials.

trend qualitatively agrees with the corresponding experimental lifetimes, which drop from 1.56 ps for $N_A = 1$ to 920 fs for $N_A = 7$.[12] Between about $N_A = 15$ and 25 a plateau of minimum lifetime τ of ca. 100 fs is reached. At $N_A = 30$ a first RIS occurs. Beyond this state the lifetime decreases again, runs through a minimum, before increasing toward even higher rotational energy. As in the DCl^+ RIS are observed for all other vibrational states. In summary, the following quantum states represent RIS: $v_A = 5$, $N_A = 43$ (4568 fs); $v_A = 6$, $N_A = 37$ (2924 fs); $v_A = 7$, $N_A = 30$ (1947 fs); $v_A = 8$, $N_A = 21$ (1254 fs) and 33 (1952 fs); $v_A = 9$, $N_A = 4$ (855 fs) and 25 (1188 fs). For the vibrational states $v_A = 8$ and $v_A = 9$ the calculated lifetimes at threshold ($N_A = 0$) are 95 and 825 fs, respectively. Again the qualitative trend of increasing lifetime with increasing v_A is also observed in the experimental values, which are 63 and 139 fs, respectively.[12] With increasing v_A the first RIS becomes lower in absolute lifetime and wider in terms of the N dependence. Qualitatively, the current results for HCl^+ agree with previous reports;[31] however, the absolute numbers differ slightly.

In analogy to the discussion of the DCl^+ results, we again replot the results for HCl^+ as the function of the energy difference between the rovibrational energy and the crossing energy between the rotronic potentials of the A state and the repulsive $^4\Pi$ state (cf. Figure 5).

Similar to the case for DCl^+ in Figure 5, several RIS occur at very similar ΔE_c for HCl^+. More specifically, the first RIS is observed around $\Delta E_c = 0.0065$ au for $v_A = 5$ and $v_A = 6$ and $\Delta E_c = 0.0060$ au for $v_A = 7-9$. A second RIS occurs for $v_A = 9$ and 10 at almost identical ΔE_c values (0.0105 au). There is a qualitative trend of increasing ΔE_c for decreasing v_A in the first RIS but increasing ΔE_c for increasing v_A for the second RIS. For $v_A = 8$ and $v_A = 9$ two RIS are observed, with the second RIS showing a higher lifetime and a narrower width similar to the observation for DCl^+ (cf. Figure 3).

III.2. Decay of "Eigenstates" with Optical Excitation. All results presented above have been obtained by starting from $|\Psi_A(r,t)|^2 = 1$ without taking into account the optical excitation from the ion ground state. From the experimental point of view the process of bringing the population from the X state into the A state and the beginning of spin−orbit coupling cannot be separated. Particularly for very fast predissociation dynamics, the process of populating the A state, e.g., by a short laser pulse, could in principle have an effect on the dynamics and the

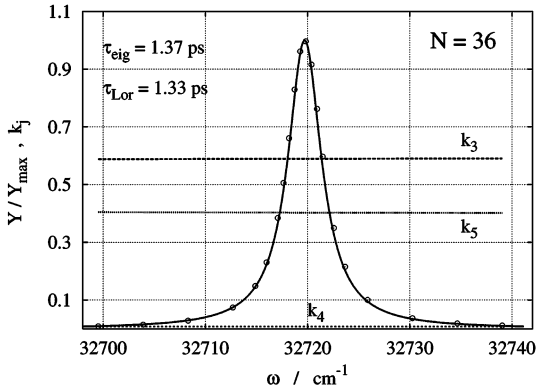

Figure 6. Product yield spectrum obtained via the final state $v_A = 8$, $N_A = 36$ of DCl^+: (symbols) numerical data; (line) Lorentzian function. Relative contribution of the three repulsive states to the overall predissociation process as a function of the excitation frequency (labeled k_3, k_4, and k_5).

multichannel interactions. In the following we address the question whether this optical excitation has a significant effect on the calculated lifetimes, i.e., whether it needs to be taken into account. For this we have solved the time dependent Schrödinger equation given in eq 1−5 (see above) with the appropriate transition dipole moments and the laser field as described in eq 9.

As will become obvious below, these calculations are more time-consuming than the free decay of eigenstate approach. Because of this difference in the required computation time, we decided to focused on three characteristic regions of the predissociation dynamics, (i) the threshold region with relatively slow decay, (ii) the region of fastest decay, and (iii) the region of a RIS with again very slow decay. At first glance one might expect that taking into account optical excitation is more important in region ii than in region iii. As we will show below, this is not the case.

The current test calculations with optical excitation have been performed for the $v_A = 8$ state in the DCl^+ ion. In the following we present lifetimes obtained by calculating the excitation spectrum of the ions of interest, followed by fitting a Lorentzian line shape function to that spectrum and converting this to the corresponding lifetime. Obviously, any significant deviation from Lorentzian line shape would be noticed immediately.

Numerically, the excitation spectrum of the ion is obtained by summing all populations that do not reside in the electronic ground state (X state) at the end of the wave packet propagation ($1 - |\Psi_X|^2$) for different excitation frequencies. More specifically, the transitions chosen are typically of the P_1 type. We carefully checked that the results do not depend on the specific transition but are solely determined by the properties of the final state. Inherently, this approach takes into account multichannel interactions, which are key points of dynamics as opposed to classical kinetics. Figure 6 shows the product ion yield spectrum obtained via absorption leading into the $v_A = 8$, $N_A = 36$ state. Evidently, the yield spectrum obtained numerically can be well approximated by a Lorentzian line shape. Figure 6 also shows the relative contribution of the three predissociation channels k_j. These channel contributions are defined as the ratio of each individual flux $\mathrm{Flux}(\Psi_j)$ to the sum of all predissociation fluxes

$$k_j = \frac{\mathrm{Flux}(\Psi_j)}{\sum_{j=3}^{5} \mathrm{Flux}(\Psi_j)} \qquad (10)$$

TABLE 1: Calculated Predissociation Lifetimes for DCl^+ ($v = 8$) without and with Excitation Taken into Account [$N_A = 36$ (Threshold), $N_A = 46$ (Fast Decay), $N_A = 53$ (RIS), $N_A = 60$ (Fast Decay)]

N_A	without excitation	with excitation
36	1.37 ps	1.33 ps
46	93 fs	90 fs
53	1.7 ps	1.6 ps
60	411 fs	409 fs

The k_j's do not vary noticeably with the excitation frequency in this case. We note that channel no. 4 ($^2\Sigma^-$) does not contribute to the dynamics. The reason is that the corresponding rovibronic eigenstate lies below the crossing of the A $^2\Sigma^+$ state with the $^2\Sigma^-$ state (but above the crossing with the $^4\Sigma^-$ and the $^4\Pi$ states). The lifetime concluded from the width of this spectrum, $\tau = 1.33$ ps, agrees well with that obtained without the optical excitation, $\tau = 1.37$ ps (cf. Table 1).

Figure 7 presents the product yield spectrum obtained via the final DCl^+ state, $v_A = 8$, $N_A = 46$, which correlates with a region of fast decay. Here we indicate calculations with two different lengths of the laser pulse, i.e., $t_l = 20$ (×) and $t_l = 40$ ps (○). These two sets of calculations lead to almost identical results, giving evidence that the laser pulses employed were long enough. Both data sets are well represented by a Lorentzian curve, also indicated in Figure 8 (a close inspection, however, reveals deviation from a Lorentzian line shape at the 1% level). The lifetime derived from the line shape analysis is 90 fs. The

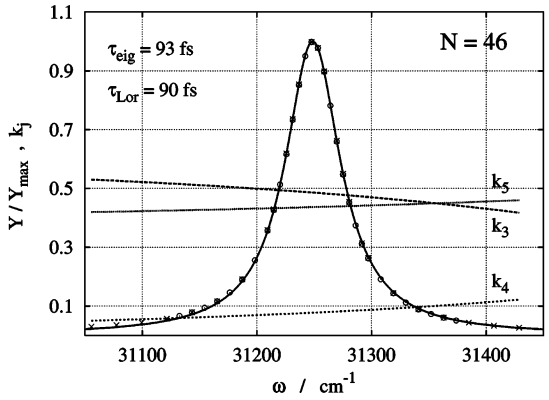

Figure 7. Product ion yield spectrum obtained via the final state $v_A = 8$, $N_A = 46$ of DCl^+: (symbols) numerical data (× = 20 ps, ○ = 40 ps); (line) Lorentzian function. Relative contribution of the three repulsive states to the overall predissociation process as a function of the excitation frequency (labeled k_3, k_4, and k_5).

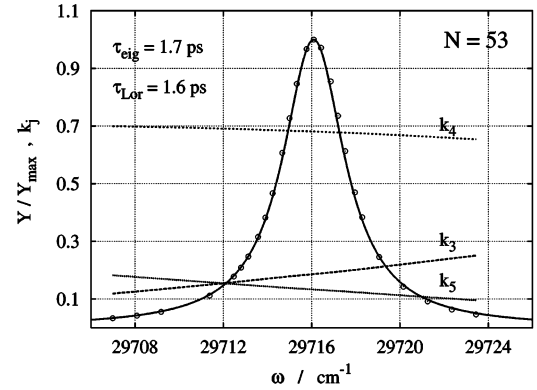

Figure 8. Product ion yield spectrum obtained via the final state $v_A = 8$, $N_A = 53$ of DCl^+: (symbols) numerical data; (line) Lorentzian function. Relative contribution of the three repulsive states to the overall predissociation process as a function of the excitation frequency (labeled k_3, k_4, and k_5).

relative contribution of the three predissociation channels varies slightly with the excitation frequency. In contrast to the threshold region (Figure 6), here all three channels contribute to the predissociation, with almost equal weight of channels 3 and 5 and about 10% contribution from channel 4. We note that channels 3 and 5 are also associated with a larger spin−orbit coupling compared to channel 4.[28] More specifically, k_4 and k_5 slightly increase with increasing laser frequency, whereas k_3 decreases. This gives evidence for multichannel interaction in the predissociation dynamics.

Finally Figure 8 shows the product yield spectrum obtained via the final DCl^+ state, $v' = 8$, $N_A = 53$, which is a RIS state. Again the results of the numerical calculation agree perfectly with a Lorentzian line shape. In contrast to the $N_A = 46$ state (Figure 7), here channel 4 clearly dominates the predissociation. Subtle differences also appear in the frequency dependence of the channel yields. Here, the contributions of k_4 and k_5 decrease with increasing frequency, whereas k_3 increases. Again the observation of frequency dependent channel yields—in particular the difference between $N_A = 53$ and $N_A = 46$—directly reflects the dynamical character of multichannel interactions, which would not be easily accounted for in a classical kinetic description.

As briefly indicated above, our wave packet propagation includes the analysis of the time dependence of populations in all electronic states considered and also the individual flux given in eq 10. Here, we wish to emphasize that for all product channels the flux increases monotonically with time. Oscillations of population are not observed under the current conditions. We also note that a transient population appears in the A state. At the end of the laser pulse this population decreases to zero again and all population is in the products.

Table 1 lists a comparison of the calculated predissociation lifetimes with and without optical excitation for the states $v_A = 8$, $N_A = 36$ (i, threshold), $v_A = 8$, $N_A = 46$ (ii, fast decay), $v_A = 8$, $N_A = 53$ (iii, RIS), and $v_A = 8$, $N_A = 60$ (ii, again fast decay). The latter is included because it is the last quasi-bound state below the top of the centrifugal barrier T_4, for which the yield of direct dissociation (leading to formation of H^+) is below 1%. For even higher rotational states direct dissociation can effectively compete with predissociation. This will be the subject of future work.[39]

The results show almost numerical agreement for the two cases of fast decay and still very good agreement to within about 5% for the two cases of slow decay (threshold and RIS). These results prove that taking into account the optical excitation is not intrinsically important for representing correct predissociation lifetimes. The reason the calculated lifetimes differ in the case of slow decay is not related to any possible shortcoming of the free decay approach. It is rather related to the effect that the lifetimes in the region of a RIS strongly depend on the absolute energy of the molecule. This energy, however, is slightly shifted when the optical excitation is included. This shift occurs for both slow and fast decaying states; however, it only becomes relevant for the RIS, because only there does the lifetime change significantly with absolute energy. We will come back to this point below. Overall, the calculations provide evidence that the "free decay of eigenstate" model presented in the first part of this work gives reliable results. We also emphasize that calculations for HCl^+ lead to very similar conclusions regarding the reliability of the free decay approach.

IV. Discussion

In the previous section we have shown that the RIS in HCl^+ and DCl^+ are periodic features. The question remains, what is

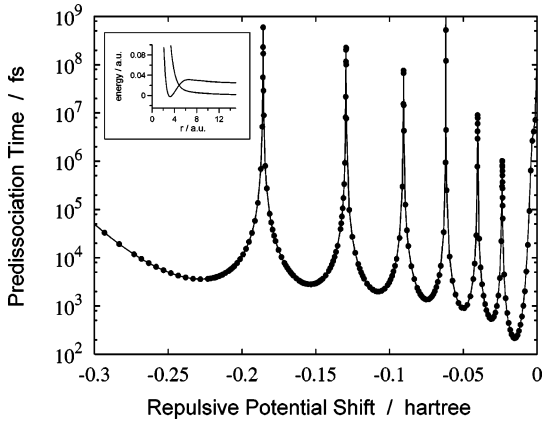

Figure 9. Predissociation lifetime of the HCl^+ as a function of the shift between the bound and a single repulsive state. The reference energy is the predissociation limit of the ion.

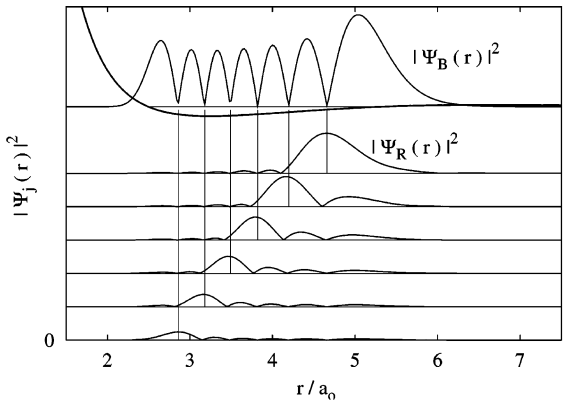

Figure 10. Bound state potential for the HCl^+ together with the square of the wave function of the bound state $|\Psi_B|^2$ and of the model repulsive state $|\Psi_R|^2$ for six different relative positions of bound and repulsive states. For further explanation see the text.

the molecular origin of the RIS, and what are the vibrational state specific characteristics of the RIS? This is connected to the question for the maximum number of RIS possible in a given vibrational state. Clearly, energetic periodicities exist, which appear to result from unfavorable interaction of the bound A state with each of the repulsive states. A closer inspection indicates multichannel interaction. Here the actual situation including three repulsive states certainly leads to smearing out the effect of the RIS. The signature of the RIS is expected to be more pronounced for the situation of only one repulsive curve crossing with one bound curve. To further investigate the molecular origin of the RIS, we have performed model calculations with just two potential curves. This situation is obtained by simply dropping two states ($j = 3, 4$) from the calculations described above. Because taking into account optical excitation was not found to be crucial for HCl^+ and DCl^+, we also go back to the model of free decay of an eigenfunction. We then continuously shift the repulsive state potential from the dissociation limit of the bound state (shift = 0) down to the minimum of the bound state potential (cf. inset of Figure 9). For each relative position the predissociation lifetime is calculated and plotted in Figure 9. More specifically, the calculations are performed starting from $\upsilon_A = 6$ and $N_A = 37$ in the HCl^+ ion.

Besides from a threshold region for shift = 0, Figure 9 exhibits a total of six maxima in the predissociation lifetime, i.e., RIS. The maximum lifetime in these RIS is much larger than those discussed in the Results. The main reason is we here consider a basically continuous shift of the relative position, whereas we were restricted to real molecular eigenstates in the calculations of the first part of this work. A minor effect is that the RIS due to a specific channel are not smeared out by a neighboring channel in this model. Again, the absolute value of the maximum lifetime is not the aim of this work. Studying the relevant nuclear wave functions, however, turns out to be very instructive. In Figure 10 we show the bound state potential together with the square of the corresponding nuclear wave function in the A state, $|\Psi_B|^2$ (B = bound). Because it is a $\upsilon = 6$ state, we observe 6 nodes. Furthermore, Figure 10 includes the square of the nuclear wave function of the repulsive state, $|\Psi_R|^2$ (R = repulsive), for six different energetic positions corresponding to the six RIS observed in Figure 10. For better illustration these wave functions are shifted on the vertical energy axis. The important point to note is that, for each $|\Psi_R|^2$, its maximum value coincides with an internuclear distance, where $|\Psi_B|^2$ exhibits a node. Thus, the condition for observing a RIS requires that the overlap between the bound state wave function and the repulsive state wave function is unfavorable. Basically, this condition needs to be met at all times. If this overlap is favorable at any time, the zero-order eigenstate will decay. By careful variation of the model conditions we have validated the reasoning presented above. For example, using a different starting point for shifting the potentials just leads to a shift of all the RIS. Decreasing the spin−orbit coupling by a factor of 5 changes the absolute lifetimes, but not the position of the RIS, as expected.

The analysis presented above is able to rationalize the origin of the RIS. In fact, there are other published reports of related observations in the predissociation of diatomic molecules,[14,22,40−44] sometimes referred to as fragmentary rotational structure. It is interesting to note, however, that the literature examples all refer to the situation of crossing between just two potentials, which we just discussed as a simplification of the more complex situation in DCl^+ predissociation. In the case of interaction between two potentials, oscillation of lifetimes can in principle be rationalized by frequency domain and time domain models. Basically, both models point at the phase relation between the relevant wave functions. Inherently, models based on stationary wave functions cannot reflect their time evolution. That, however, is important in fast predissociation processes such as in HCl^+ and even moreso in HBr^+.[27,28]

We finally come back to the true situation in DCl^+ and HCl^+, with the presence of three instead of just one repulsive state. Here, the perhaps surprising observation is RIS also occur in a multichannel system without being completely smeared out. For illustration, Figure 11 presents the rotronic potentials of all five electronic states involved in the predissociation of DCl^+, $\upsilon_A = 8$, $N_A = 46$ (fast decay), together with the corresponding wave functions. Evidently, both the internuclear distance at which the states cross and the crossing energy differ slightly for the three repulsive states. However, the square of the wave functions of the three repulsive states all exhibit a maximum, where also the square of the bound state wave function exhibits a maximum. The current picture corresponds to time $t = t_l/2$; however, we emphasize that very similar results are obtained at all other times.

For comparison Figure 12 shows the analogous situation for DCl^+, $\upsilon_A = 8$, $N_A = 53$ (RIS). Here $|\Psi_3|^2$ and $|\Psi_5|^2$ exhibit maxima exactly where $|\Psi_A|^2$ exhibits a minimum, whereas the maximum of $|\Psi_4|^2$ basically coincides with that of $|\Psi_A|^2$. The former favors slow decay and is in fact the reason this state is a RIS. The latter would in principle favor fast decay. This is

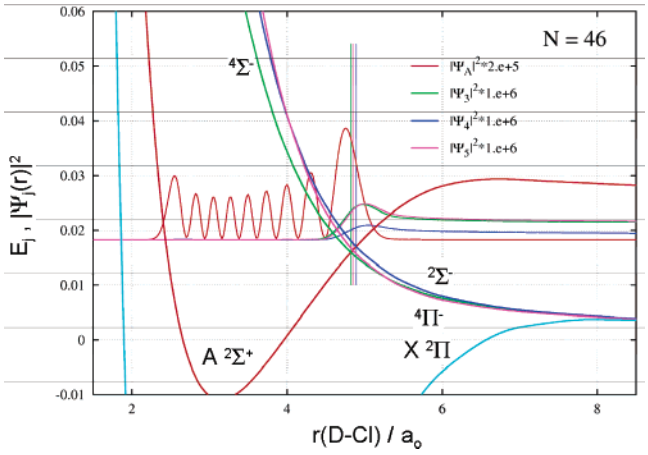

Figure 11. Rotronic potentials for DCl^+ $v_A = 8$, $N_A = 46$, together with the square of the wave function of the bound state $|\Psi_A|^2$ and of the repulsive state $|\Psi_j|^2$ ($j = 3-5$). Vertical lines indicate the crossing of bound A potential and repulsive potentials $j = 3-5$. For further explanation see the text.

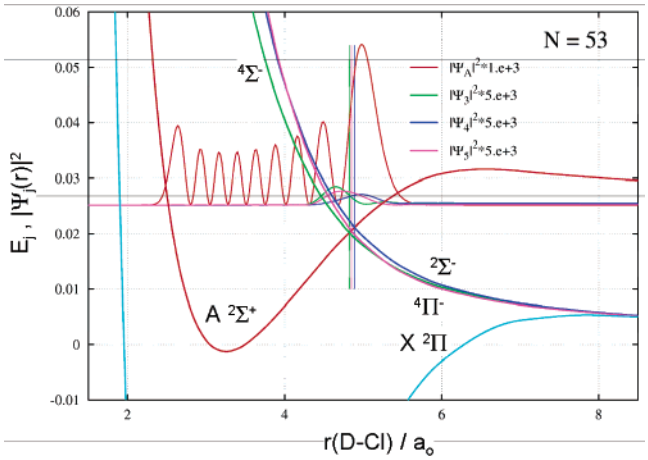

Figure 12. Rotronic potentials for DCl^+ $v_A = 8$, $N_A = 53$, together with the square of the wave function of the bound state $|\Psi_A|^2$ and of the repulsive state $|\Psi_j|^2$ ($j = 3-5$). For further explanation see the text.

indeed in agreement with Figure 8, where k_4 was observed to account for 70% of the predissociation yield. However, still channel 4 does not appear to be effective enough for destroying the RIS characteristics completely.

V. Summary

We have investigated the predissociation lifetimes of HCl^+ and DCl^+ in several rovibrational states of the electronic A $^2\Sigma^+$ state. The results show pronounced lifetime oscillations with rotational islands of stability (RIS). The maximum lifetime of the RIS appears to be higher in HCl^+ compared to DCl^+; however, the minimum lifetime is smaller in HCl^+. In other words, the contrast of lifetimes is larger in HCl^+. At the threshold of predissociation, the calculated lifetime is also larger in HCl^+. The calculated lifetimes presented in this work are in qualitative agreement with experimental data where available.

We have shown that the RIS are characterized by a common energy difference between the rovibronic energy and the zero-order crossing of rotronic states. More specifically, RIS are observed for $\Delta E_c \approx 0.006$ au and $\Delta E_c \approx 0.0105$ au in HCl^+ but $\Delta E_c \approx 0.0055$ au and $\Delta E_c \approx 0.0085$ au in DCl^+. The frequency domain period of the RIS in the ΔE_c domain is thus smaller in DCl^+ than in HCl^+. We found the ratio of these two periods of RIS to be close to the ratio of the square root of reduced masses of DCl^+ and HCl^+, i.e., the ratio of vibrational frequencies. Our current calculations, explicitly taking into account optical excitation, led to Lorentzian line shapes. These are associated with single time constants, which in turn reflect first-order kinetics. The observation of frequency dependence in the individual channel contributions, however, reflects the dynamical character of multichannel interactions.

Experimental observation of the RIS described in this work requires access to a wide range of rotational states. The lowest rotational quantum numbers for which clear RIS are predicted are $N = 17$ in DCl^+ (Figure 2) and $N = 21$ in HCl^+ (Figure 4). The relevant states are easily accessible for diatomic molecules with small rotational constants, e.g., ICl.[41] In DCl, experiments with $N = 17$ should be possible at modest temperatures of about 500 K. Thermal experiments with HCl would require even higher temperatures of about 1000 K. However, we also note that the preparation of Cl_2 in extremely high rotational states (up to $N = 420$) has been realized by the application of two counter-rotating circularly polarized fs laser pulses.[45] We hope that the current investigation stimulates future experimental work along this question.

Acknowledgment. Financial support by INTAS (project no. 03-50-5765) and by the DFG is gratefully acknowledged. We also wish to thank Joern Manz for support of this work. K.-M.W. acknowledges many fruitful and encouraging discussions with Prof. Jürgen Troe.

References and Notes

(1) Troe, J. *Z. Phys. Chem. (Muenchen, Germany)* **2003**, *217*, 1303−1317.
(2) Troe, J. *Chem. Rev.* **2003**, *103*, 4565−4576.
(3) Moller, K. B.; Henriksen, N. E.; Zewail, A. H. *J. Chem. Phys.* **2000**, *113*, 10477−10485.
(4) Zewail, A. H. *J. Phys. Chem. A* **2000**, *104*, 5660−5694.
(5) Gaspard, P.; Burghardt, I. *Chemical Reactions and Their Control on the Femtosecond Time Scale*; XXth Solvay Conference an Chemistry; John Wiley & Sons: New York, 1997.
(6) Sundstroem, V. *Femtochemistry and Femtobiology: Ultrafast Reaction Dynamics at Atomic-Scale Resolution*; Nobel Symposium 101; Imperial College Press: London, 1997.
(7) Dantus, M.; Zewail, A. *Chem. Rev.* **2004**, *104*, 1717−1718.
(8) Shapiro, M.; Brumer, P. *Principles of quantum control of molecular processes*; Wiley: Hoboken, NJ, 2003.
(9) Rice, S. A. *Nature* **2001**, *409*, 422−426.
(10) Rice, S. A.; Zhao, M. *Optimal Control of Molecular Dynamics*; Wiley-VCH: Weinheim, 2001.
(11) Michel, M.; Korolkov, M. V.; Weitzel, K. M. *Phys. Chem. Chem. Phys.* **2002**, *4*, 4083−4086.
(12) Michel, M.; Korolkov, M. V.; Weitzel, K. M. *J. Phys. Chem. A* **2004**, *108*, 9924−9930.
(13) Lefebvre-Brion, H.; Field, R. W. *The Spectra and Dynamics of of Diatomic Molecules*; Academic Press: New York, 2004.
(14) Child, M. S.; Lefebvre, R. *Chem. Phys. Lett.* **1978**, *55*, 213-216.
(15) Child, M. S.; Lefebvre, R. *Mol. Phys.* **1977**, *34*, 979−985.
(16) Sink, M. L.; Bandrauk, A. D.; Lefebvre, R. *J. Chem. Phys.* **1980**, *73*, 4451−4459.
(17) Bauschlicher, C. W., Jr.; Langhoff, S. R. *J. Chem. Phys.* **1987**, *87*, 4665−4672.
(18) Lee, S.; Freed, K. F. *J. Chem. Phys.* **1987**, *87*, 5772−5780.
(19) Banichevich, A.; Klotz, R.; Peyerimhoff, S. D. *Mol. Phys.* **1992**, *75*, 173−188.
(20) Parlant, G.; Yarkony, D. R. *J. Chem. Phys.* **1999**, *110*, 363−376.
(21) Yarkony, D. R. *J. Chem. Phys.* **1992**, *97*, 1838−1849.
(22) Sohlberg, K.; Yarkony, D. R. *J. Chem. Phys.* **1997**, *106*, 6607−6611.
(23) Kalyanaraman, C.; Sathyamurthy, N. *Chem. Phys.* **1994**, *187*, 219−226.
(24) Marquetand, P.; Engel, V. *Phys. Chem. Chemi. Phys.* **2005**, *7*, 469−474.
(25) Farias, P. M. A.; Longo, R. L. *Int. J. Quantum Chem.* **2004**, *97*, 944−948.

(26) Leonard, C.; Le Quere, F.; Peterson, K. A. *Phys. Chem. Chem. Phys.* **2005**, *7*, 1694−1699.
(27) Korolkov, M. V.; Weitzel, K. M. *Chem. Phys.* **2000**, *252*, 209−219.
(28) Korolkov, M. V.; Weitzel, K. M.; Peyerimhoff, S. D. *Int. J. Mass Spectrom.* **2000**, *201*, 109−120.
(29) Yencha, A. J.; Cormack, A. J.; Donovan, R. J.; Hopkirk, A.; King, G. C. *Chem. Phys.* **1998**, *238*, 109−131.
(30) Yencha, A. J.; Cormack, A. J.; Donovan, R. J.; Lawley, K. P.; Hopkirk, A.; King, G. C. *Chem. Phys.* **1998**, *238*, 133−151.
(31) Korolkov, M. V.; Weitzel, K. M. *Chem. Phys. Lett.* **2001**, *336*, 303−310.
(32) Pradhan, A. D.; Kirby, K. P.; Dalgarno, A. *J. Chem. Phys.* **1991**, *95*, 9009−9023.
(33) Feit, M. D.; Fleck, J. A.; Steiger, A. *J. Comput. Phys.* **1982**, *47*, 412.
(34) Korolkov, M. V.; Schmidt, B. *Chem. Phys. Lett.* **2002**, *361*, 432−438.
(35) Korolkov, M. V.; Paramonov, G. K. *Phys. Rev. A: At., Mol. Opt. Phys.* **1998**, *57*, 4998−5001.
(36) Bisseling, R. N.; Kosloff, R.; Manz, J. *J. Chem. Phys.* **1985**, *83*, 993.
(37) Penno, M.; Holzwarth, A.; Weitzel, K. M. *J. Phys. Chem. A* **1998**, *102*, 1927−1934.
(38) Penno, M.; Holzwarth, A.; Weitzel, K. M. *Mol. Phys.* **1999**, *97*, 43−52.
(39) Korolkov, Mikhail V.; Weitzel, Karl Michael. Unpublished work, 2005.
(40) Schaefer, S. H.; Bender, D.; Tiemann, E. *Chem. Phys.* **1984**, *89*, 65−79.
(41) Siese, M.; Baessmann, F.; Tiemann, E. *Chem. Phys.* **1985**, *99*, 467−477.
(42) Clevenger, J. O.; Harris, N. A.; Field, R. W.; Li, J. *J. Mol. Spectrosc.* **1999**, *193*, 412−417.
(43) Cornett, S. T.; Sadeghpour, H. R.; Cavagnero, M. J. *Phys. Rev. Lett.* **1999**, *82*, 2488−2491.
(44) Balakrishnan, N.; Esry, B. D.; Sadeghpour, H. R.; Cornett, S. T.; Cavagnero, M. J. *Phys. Rev. A* **1999**, *60*, 1407−1413.
(45) Karczmarek, J.; Wright, J.; Corkum, P.; Ivanov, M. *Phys. Rev. Lett.* **1999**, *82*, 3420−3423.